Quantum path control and isolated attosecond pulse generation with the combination of two circularly polarized laser pulses

Chang-Long Xia and Xue-Shen Liu*
Institute of Atomic and Molecular Physics, Jilin University, Changchun 130012, People's Republic of China
(Received 12 December 2012; published 10 April 2013)

We theoretically investigate the quantum paths of the high-order harmonic generation (HHG) by using a left and a right circularly polarized Gaussian laser pulse with a proper time delay. When the carrier phase of the two pulses is $\varphi_1 = 0$, $\varphi_2 = 0.5\pi$, the "gating" structure of the combined laser field disappears. The numerical results indicate that no "gating"-structure-combined laser pulse can control the quantum path. The HHG process is investigated by the semiclassical three-step model that makes use of a finite initial transverse velocity in the elliptically polarized field. For the case of $\lambda_1 = 800$ nm, $\lambda_2 = 1600$ nm, only a short quantum path contributes to the HHG, and an isolated attosecond pulse would be obtained. For the case of $\lambda_2 = 1600$, $\varphi_2 = 0.5\pi$, a supercontinuum spectrum plateau from 180 to 570 eV which includes the water window region is obtained, and attosecond pulses with the duration of about 75 as and a tunable central wavelength could be generated by superposing a bandwidth of 50 eV in the plateau area.

DOI: 10.1103/PhysRevA.87.043406 PACS number(s): 32.80.Rm, 42.65.Ky

Isolated attosecond pulse (IAP) generation has been a hot topic due to its potential applications, such as probing and controlling the electron motions inside atoms, molecules, and solids; tracing the bound electron motion; and so on [1]. So far the high-order harmonic generation (HHG) is the most promising approach to synthesize an attosecond pulse. The HHG, which is generated by an intense laser field interacting with atoms or molecules, can be described by a three-step model [2]: tunnel ionization of the atom or molecule, acceleration of the resulting electron, and the recombination of the electron with the parent ion by releasing an energetic photon of energy. The central frequency of the produced attosecond pulses has been limited to the extreme-uv to soft-x-ray domain, but the so-called water window, from 2.3 to 4.4 nm (from 550 to 280 eV), will be more useful in detecting and controlling ultrafast processes with unprecedented resolution, such as core-level dynamics and the imaging of live cells [3,4]. To generate a tunable IAP, we need to produce a broadband supercontinuous harmonics with low interferences of the quantum paths and a high stabilizing phase of the HHG.

A number of schemes have been introduced to produce IAP, such as the few-cycle pulse [5,6], two-color fields [7–10], two-color fields with a static electric field or xuv pulse [11,12], and so on. The strong dependence of HHG efficiency on the ellipticity of the driving field gives us another way to control the IAP generation. The polarization gating (PG) scheme [13–15], which can be obtained by combining two counterrotating, circularly polarized laser pulses with a proper delay, has been proposed to generate the xuv supercontinumm and single attosecond pulse. Furthermore, the double optical gating (DOG) [16–18] and generalized DOG (GDOG) [19] have been also proposed to generate the IAP. The carrier frequency and the carrier envelope phase of the two circularly polarized pulses used in the PG scheme is always the same. The scheme by combining two circularly polarized laser fields with frequencies ω and 2ω was investigated both experimentally [20] and theoretically [21,22].

In this paper, based on the single-active approximation, the HHG and IAP can be investigated by solving the two-dimensional time-dependent Schrödinger equation with the second-order splitting-operator fast Fourier transform algorithm, the details can found in our previous work [11]. In our simulation, we choose a soft-core Coulomb potential model $V(x,y) = -b/\sqrt{x^2+y^2+a^2}$ and set $b = 1.5$, $a^2 = 0.6$ corresponding to the binding energy of 0.9 a.u. for the ground state of a helium atom. The combination of the pulse with a time-dependent ellipticity is generated by the superposition of a left and a right circularly polarized Gaussian pulse, which is similar to the PG scheme, but the carrier frequency or the carrier envelope phase may be different. The electric fields of the left and right circularly polarized pulses propagating in the z direction are

$$E_l(t) = E_0 f(t - T_d/2.0)[\hat{x}\cos(\omega_1 t + \varphi_1) + \hat{y}\sin(\omega_1 t + \varphi_1)], \tag{1}$$

$$E_r(t) = E_0 f(t + T_d/2.0)[\hat{x}\cos(\omega_2 t + \varphi_2) - \hat{y}\sin(\omega_2 t + \varphi_2)], \tag{2}$$

where E_0 is the peak field amplitude, $f(t) = \exp[-2\ln(2)t^2/\tau^2]$ is the envelope of the laser field, $\tau = 5$ fs is the pulse duration, and $T_d = 4$ fs is the time delay between two pulses. $\omega_{1,2}$ and $\varphi_{1,2}$ are the frequencies and the carrier envelope phases of the two pulses, the $\hat{x}$ and $\hat{y}$ are unit vectors in the x and y directions, respectively. The electric field of the combined pulse is $\vec{E}(t) = \hat{x}E_x + \hat{y}E_y$, and

$$E_x(t) = E_0[f(t - T_d/2.0)\cos(\omega_1 t + \varphi_1) + f(t + T_d/2.0)\cos(\omega_2 t + \varphi_2)], \tag{3}$$

$$E_y(t) = E_0[f(t - T_d/2.0)\sin(\omega_1 t + \varphi_1) - f(t + T_d/2.0)\sin(\omega_2 t + \varphi_2)]. \tag{4}$$

The HHG can be well explained by the semiclassical three-step model. The trajectories favorable for HHG can be found

*Corresponding author: liuxs@jlu.edu.cn

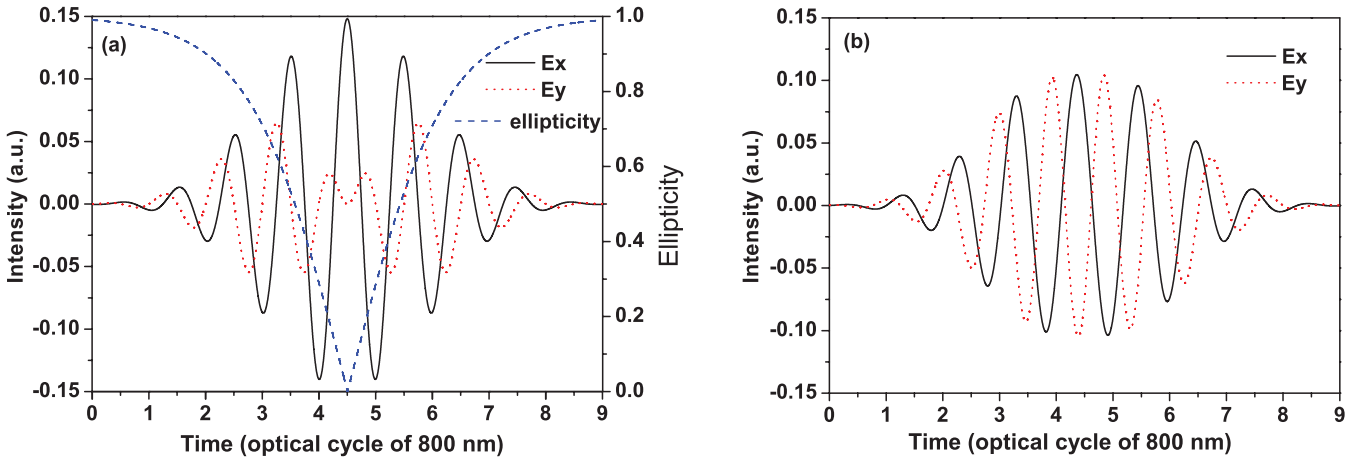

FIG. 1. (Color online) The electric field of the laser pulse with the combination of a left and a right circularly polarized Gaussian pulse. (a) $\varphi_1 = \varphi_2 = 0$, (b) $\varphi_1 = 0, \varphi_2 = 0.5\pi$.

easily when the Coulomb field of the ion is neglected, and the initial positions x_0 and y_0 are set to zero according to the three-step model [23–25], so the trajectory can be written as

$$x(t) = \int_{t_0}^{t} \left[\int_{t_0}^{t'} E_x(t'')dt'' + v_{x0} \right] dt', \tag{5}$$

$$y(t) = \int_{t_0}^{t} \left[\int_{t_0}^{t'} E_y(t'')dt'' + v_{y0} \right] dt'. \tag{6}$$

Kopold *et al*. [26] indicated that if the electron starts with zero velocity it never returns to its origin. The transverse displacement caused by the external field is compensated by an initial transverse velocity in the elliptically polarized field [23,26]. Thus the high-order harmonic is generated by the electron trajectories with nonzero initial velocity. As the electron leaves the atom by the tunneling, the initial velocity parallel to the ionizing field can be set to zero. The initial velocities can be written as $v_{x0} = v_0 \sin\alpha_0$ and $v_{y0} = v_0 \cos\alpha_0$, where v_0 is the initial velocity transverse to the ionizing field and α_0 is the angle between the ionizing filed vector and the coordinate axis at the ionization time t_0. The recombination time with a proper finite initial velocity will be obtained by solving $x(t) = 0$ and $y(t) = 0$, then we would get the trajectory and the kinetic energy at the recombination time.

First, we set the phases, the frequencies, and the intensities of the two circularly polarized pulses to be the same, i.e., $\varphi_1 = \varphi_2 = 0$, $\omega_1 = \omega_2 = 0.057$ a.u. (800 nm in wavelength) and $I_0 = 3 \times 10^{14}$ W/cm^2. The combined electric fields of the two pulses are shown in Fig. 1(a), which is the PG scheme as discussed by the authors of Ref. [14]. As indicated in Ref. [14], the harmonic signal drops quickly as the ellipticity increases, and the middle temporal range with the ellipticity less than 0.2 can be viewed as a gate, where the electric field is almost linearly polarized. The high-order harmonic spectrum with modulations on the plateau area is shown by the solid black line in Fig. 2, and the cutoff is about 175 eV. As we know, the modulations come from the interferences of the different quantum paths, and it is not propitious for generating an isolated attosecond pulse.

Second, we set $\varphi_1 = 0, \varphi_2 = 0.5\pi$, and the other parameters are the same as those in Fig. 1(a). The combined electric fields of the two pulses are shown in Fig. 1(b), which indicates that the "gating" structure disappears and the electric field looks like an orthogonal laser field. The maximum strength of the pulse is less than that of the case of $\varphi_1 = \varphi_2 = 0$. The high-order harmonic spectrum with fewer modulations on the plateau area is shown by the dotted (red) line in Fig. 2, and the cutoff is about 160 eV. Therefore no "gating"-structure-combined laser field may control the quantum path.

To further understand the physical mechanism of the two schemes, we investigate the emission time of harmonics in terms of the time-frequency analysis [27]. The time-frequency distributions of the HHG corresponding to the solid black and the dotted (red) lines in Fig. 2 are shown in Figs. 3(a) and 3(b), respectively. As shown in Fig. 3(a), two photon energy peaks, which are labeled as A_1 and B_1, contribute to the HHG. Both the long and short quantum paths came out in A_1 and B_1. The intensity of B_1 is weaker than that of A_1, and the intensity of the long path of B_2 is weakest compared to that of the other

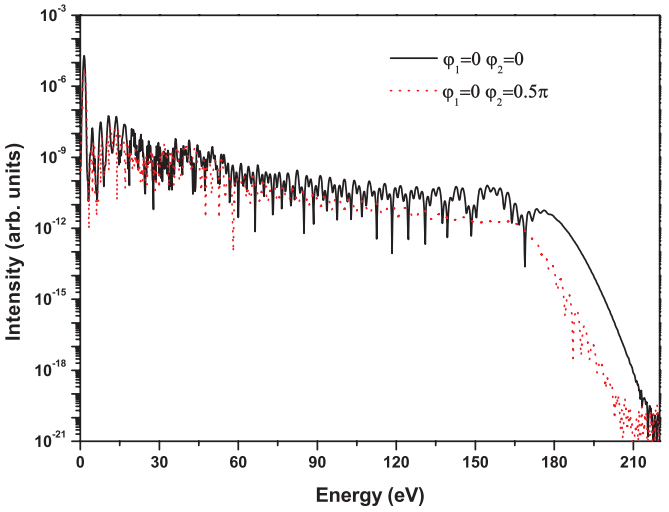

FIG. 2. (Color online) High-order harmonic spectrum produced from the combined laser field. The cases of $\varphi_1 = \varphi_2 = 0$ and $\varphi_1 = 0$, $\varphi_2 = 0.5\pi$ are shown by the solid black line and dotted (red) line, respectively.

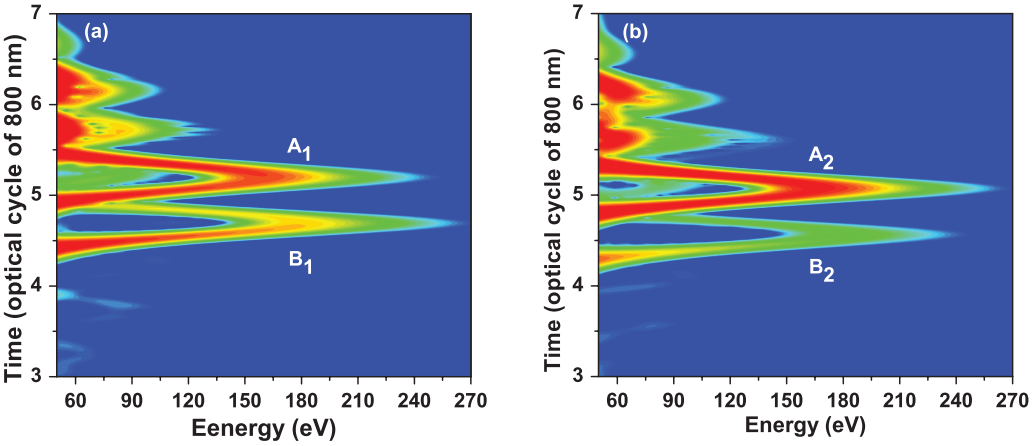

FIG. 3. (Color online) Time-frequency distributions of the HHG corresponding to (a) the solid black line in Fig. 2 ($\varphi_1 = \varphi_2 = 0$) and (b) the dotted (red) line in Fig. 2 ($\varphi_1 = 0$, $\varphi_2 = 0.5\pi$).

three paths. For the case of $\varphi_1 = 0, \varphi_2 = 0.5\pi$, Fig. 3(b) shows that there are also two photon energy peaks contributing to the HHG, but the long path of B_2 is too weak to be ignored, and the intensity of the short path of B_2 is weaker than that of A_2. The intensity of the short and long quantum paths of the peak A_2 is almost the same. The intensity of B_2 is weaker than that of B_1; this explains why the intensity of the HHG of $\varphi_1 = 0$, $\varphi_2 = 0.5\pi$ is lower than that of $\varphi_1 = 0$, $\varphi_2 = 0$. The interferences of quantum path for the case of $\varphi_1 = 0$, $\varphi_2 = 0.5\pi$ is weaker than that of the case of $\varphi_1 = 0$, $\varphi_2 = 0$, which can explain why the modulation on the plateau area of the high-order harmonic spectrum is less for the case of $\varphi_1 = 0$, $\varphi_2 = 0.5\pi$.

W also investigate the HHG process by the semiclassical three-step model. Two ionization times 4.05 and 4.55 o.c. (o.c. means optical cycle of 800 nm) were selected to describe the electron trajectory for the case of $\varphi_1 = \varphi_2 = 0$. As shown in Fig. 4(a), the electron missed the parent ion for the case of $v_0 = 0$, but a return can be achieved if the trajectory is launched with a finite initial transverse velocity v_0. Figure 4(b) shows the dependence of the energy (by summing up the kinetic energy and the binding energy) on the ionization (blue circles) and

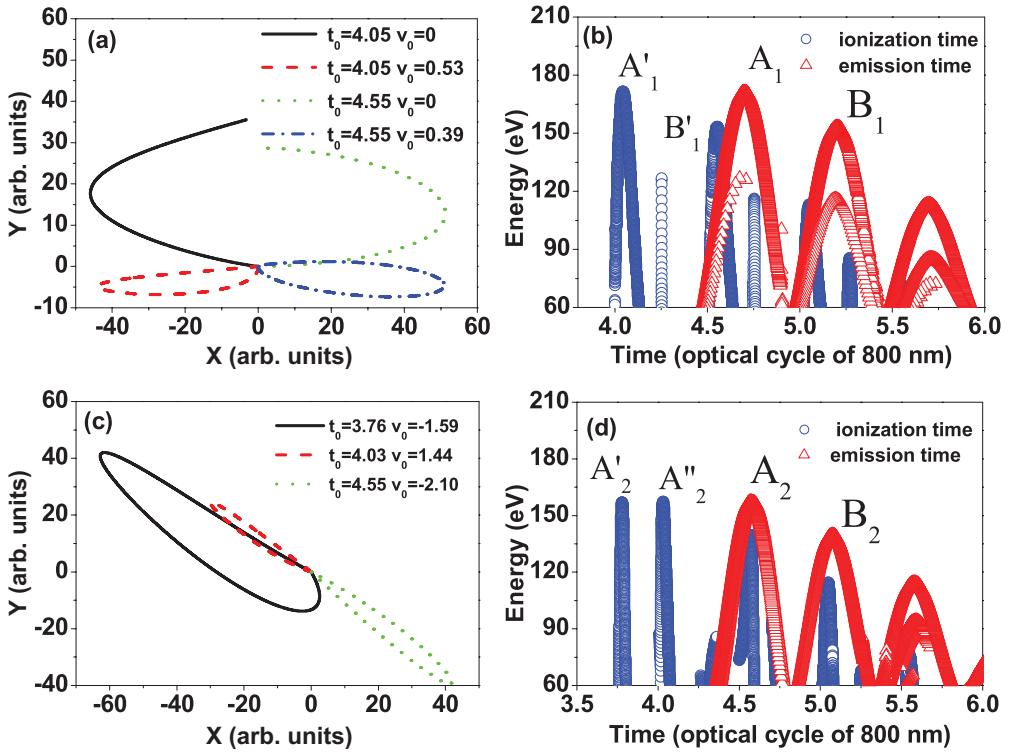

FIG. 4. (Color online) (a, c) The electron trajectories for the case of $\varphi_1 = \varphi_2 = 0$ and $\varphi_1 = 0$, $\varphi_2 = 0.5\pi$, respectively, are shown. (b, d) The dependence of the energy (by summing the kinetic energy and the binding energy) on the ionization (blue circles) and emission times (red triangles) for the cases of $\varphi_1 = \varphi_2 = 0$ and $\varphi_1 = 0$, $\varphi_2 = 0.5\pi$, respectively, are shown.

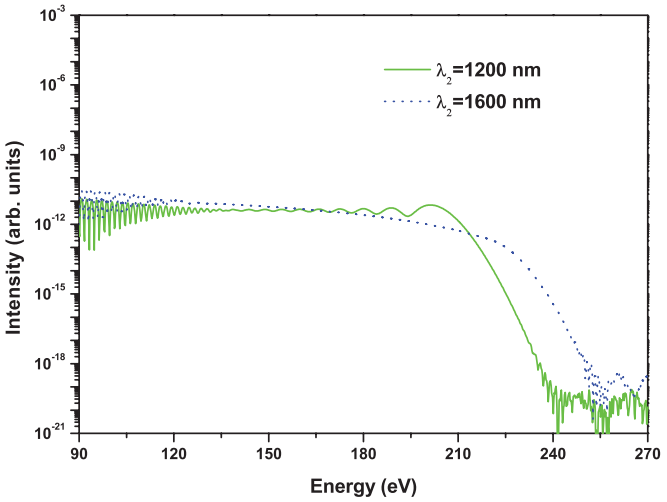

FIG. 5. (Color online) High-order harmonic spectrum produced from the combined field. The cases of $\lambda_2 = 1200$ nm and $\lambda_2 = 1600$ nm are shown by the solid (green) and the dotted (blue) lines, respectively. Other parameters are the same as those in Fig. 1(b).

emission times (red triangles) for the case of $\varphi_1 = \varphi_2 = 0$. The peak A_1 generated at about 4.7 o.c. with the energy about 175 eV and the peak B_1 generated at about 5.2 o.c. with the energy 155 eV. For the case of $\varphi_1 = 0, \varphi_2 = 0.5\pi$, the electron also returned to the parent ion with proper transverse velocity, which is shown in Fig. 4(c). As shown in Fig. 4(d), one can see that two ionization peaks A_2' and A_2'' returned almost at the same time 4.6 o.c. with the energy 160 eV and the peak B_2 generated at about 5.1 o.c. with the energy 150 eV. These results correspond to the discussion of Fig. 3.

We change the wavelength of the right circularly polarized pulse to 1200 nm, keeping the other parameters the same as those in Fig. 1(b), and investigate the HHG and IAP generation. A supercontinuum harmonic plateau with the cutoff of 200 eV is obtained as shown by the solid (green) line in Fig. 5. When the wavelength of the right circularly polarized pulse is changed to 1600 nm, the cutoff of the HHG extends to 220 eV and the bandwidth of the supercontinuum harmonic plateau is about 100 eV as shown by the dotted (blue) line in Fig. 5.

We also investigate the time-frequency distribution of these two cases. For the case of $\lambda_2 = 1200$ nm, Fig. 6(a) shows that there are two photon energy peaks A_3 and B_3, which contribute to the harmonic plateau. The energy of B_3 is about 130 eV which corresponds to the end of the modulations of HHG, and the intensity of the long path of A_3 is weaker than that of the short path, so the supercontinuum harmonic plateau is mainly contributed to by the short path of A_3. For the case of $\lambda_2 = 1600$ nm, Fig. 6(b) shows that there is only a short path in peak A_4, which contributes to the supercontinuum harmonic plateau and is beneficial in generating an IAP. The intensity of the peak B_4, which only contributes to the harmonics under the 120 eV, is weak. Only one path contributes to the plateau of the harmonic spectrum, which corresponds to the conclusions of the authors of Refs. [21,22]. By comparing the quantum paths and the harmonic spectrum, we found that the smooth spectrum plateaus shown in Fig. 5 are mainly contributed to by the quantum paths A_3 or A_4 shown in Fig. 6. The interference in the process can be called the intracycle interference. The spectrum plateaus with the modulations shown in Fig. 2 are mainly contributed to by the quantum path A_1, B_1 and path A_2, B_2 shown in Fig. 3. The interference in the process can be called the intercycle interference. The intracycle interference generates the shape and structure of the harmonic, while the intercycle interference generates discrete harmonics, which corresponds to the statement in Ref. [28].

We investigate the attosecond pulse generation, which can be obtained by superposing several orders of the harmonics. The temporal envelopes are obtained by summing up the intensities of the x and the y components and normalized, which is shown in Fig. 7. For the case of $\varphi_1 = \varphi_2 = 0$ with the wavelength 800 nm, an attosecond train is obtained. Figure 7 shows that the peak P_1 of the attosecond train, which is generated at about 4.6 o.c., is mainly contributed to by peak B_1 in Fig. 3(a). The peak P_2 of the attosecond train with satellite pulses is due to the interferences of the short and long quantum paths of peak A_1 in Fig. 3(a). When the phase is changed to $\varphi_2 = 0.5\pi$ with the wavelength 800 nm, two main peaks P_3 and P_4 with less satellite pulses are obtained. The strength of peaks P_3 and P_4 of the attoseond pulses are comparable, which is because the interference by the short and long quantum paths of the peak A_2 in Fig. 3(b) is weak. If the wavelength of the

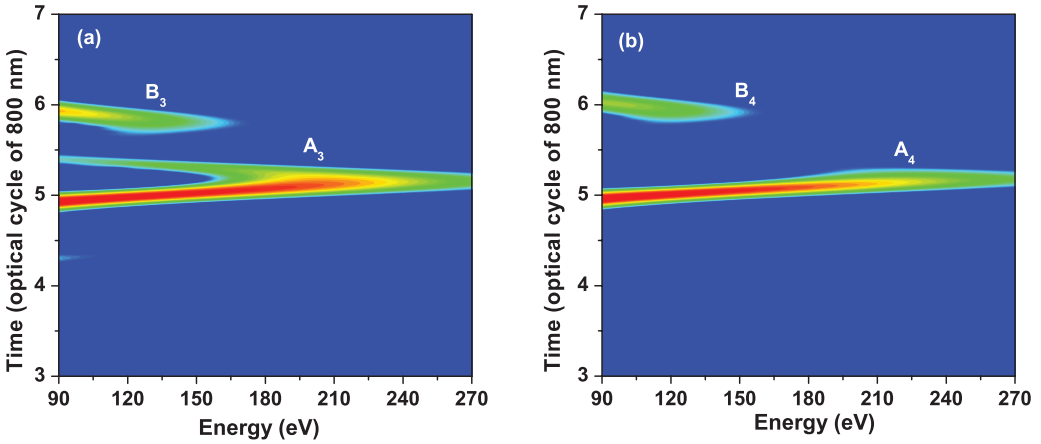

FIG. 6. (Color online) Time-frequency distributions of the HHG corresponding to (a) the solid (green) line in Fig. 5 ($\lambda_2 = 1200$ nm) and (b) the dotted (blue) line in Fig. 5 ($\lambda_2 = 1600$ nm).

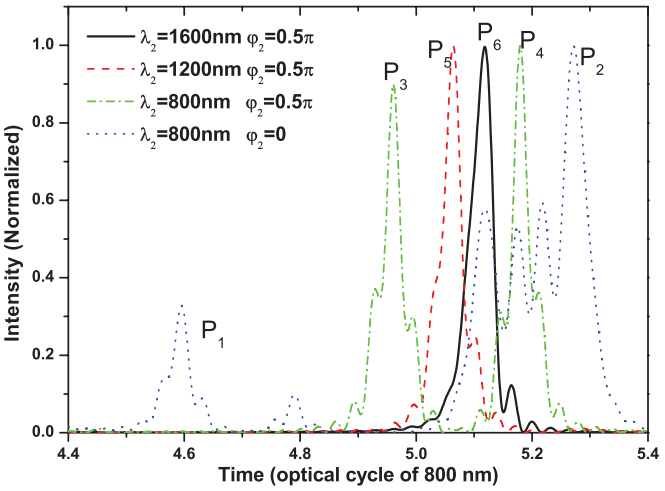

FIG. 7. (Color online) Temporal envelopes of the attosecond pulses generated in the ranges of 125–175 eV (peaks P_1 and P_2, $\varphi_2 = 0$, $\lambda_2 = 800$ nm), 110–160 eV (peaks P_3 and P_4, $\varphi_2 = 0.5\pi$, $\lambda_2 = 800$ nm), 150–200 eV (peak P_5, $\varphi_2 = 0.5\pi$, $\lambda_2 = 1200$ nm), and 170–220 eV (peak P_6, $\varphi_2 = 0.5\pi$, $\lambda_2 = 1600$ nm), respectively.

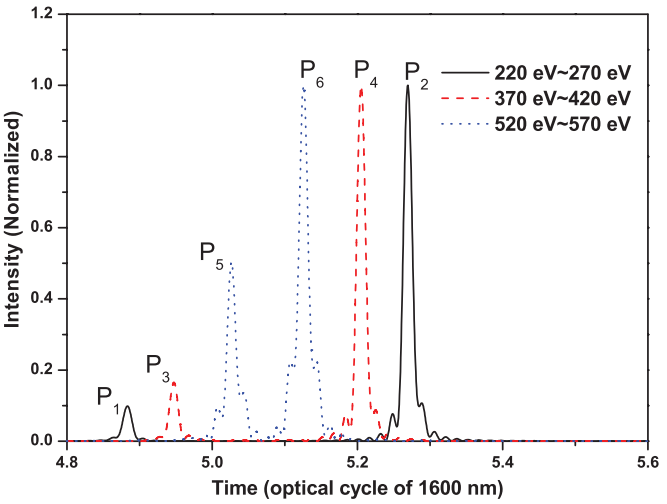

FIG. 9. (Color online) Temporal envelopes of the attosecond pulses generated in the ranges of 220–270, 370–420, and 520–570 eV, respectively, for the case of $\varphi_1 = 0$, $\varphi_2 = 0.5\pi$ with the wavelengths $\lambda_1 = \lambda_2 = 1600$ nm.

right circularly pulse is changed to 1200 nm and $\lambda_2 = 0.5\pi$, a main pulse P_5 is generated with small satellite pulses. An IAP (shown in peak P_6) with the duration of 120 as is generated for the case of $\lambda_2 = 1600$ and $\varphi_2 = 0.5\pi$, which is in agreement with the analysis in Fig. 6.

At last, we investigate the HHG and IAP when the wavelengths of the two circularly polarized pulses are 1600 nm, the durations of the two pulses are 10 fs, and the delay between the two pulses is 8 fs with the intensities being $I_0 = 3 \times 10^{14}$ W/cm^2. Figure 8(a) shows that a supercontinuum plateau which includes the whole water window region (from 180 to 570 eV) is obtained for the case of $\varphi_1 = 0$, $\varphi_2 = 0.5\pi$, and the HHG spectrum with modulations is obtained for the case of $\varphi_1 = \varphi_2 = 0$. Figure 8(b) shows the time-frequency distributions of the HHG corresponding to the case of $\varphi_1 = 0$, $\varphi_2 = 0.5\pi$. There is only a photonenergy peak A_5 that contributes to the HHG from 220 to 570 eV. The intensity of the long quantum path of A_5 is stronger than that of the short quantum path.

We investigated the attosecond pulse generation for the case of $\varphi_1 = 0$, $\varphi_2 = 0.5\pi$ and the wavelengths of the two circularly polarized pulses are 1600 nm. Figure 9 shows that a main attosecond pulse P_2 is generated, but accompanied by a weak satellite pulse P_1 by superposing the harmonics in the range of 220–270 eV, and the generation times of the two peaks are 4.88 and 5.27 o.c., which corresponds to the time-frequency analysis. Peaks P_1 and P_2 are generated by the short and the long quantum paths, respectively. When we superpose the harmonics in the range of 370–420 and 520–570 eV, which correspond to the middle and the cutoff area of the HHG plateau, the main pulses P_4 and P_6 accompanied by the satellite pulses P_3 and P_5 are generated, respectively. The generation times of the peaks P_3, P_5 and P_4, P_6 correspond to the times of the short and long quantum paths, respectively. The intensity of the satellite pulse is higher near the cutoff area, which is because the strength ratio of the short path and

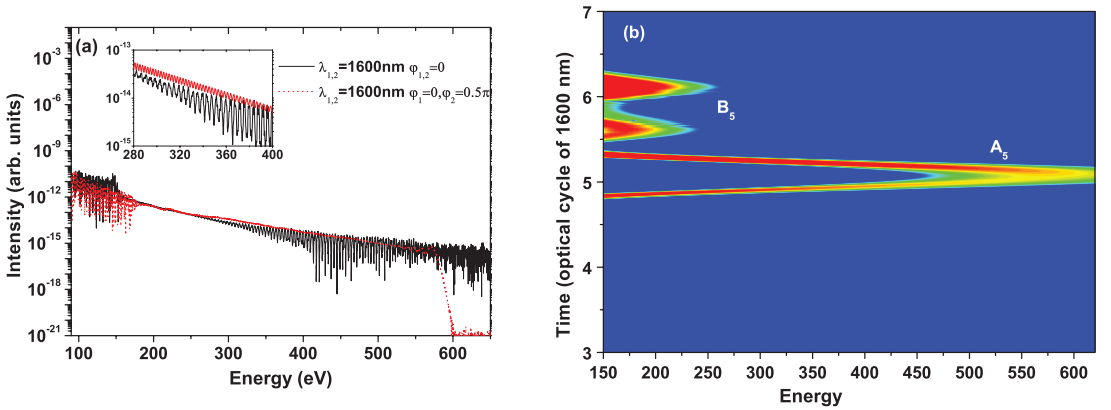

FIG. 8. (Color online) (a) High-order harmonic spectrum produced from the combined field. The cases of $\varphi_1 = 0$, $\varphi_2 = 0$ and $\varphi_1 = 0$, $\varphi_2 = 0.5\pi$, with the wavelengths $\lambda_1 = \lambda_2 = 1600$ nm are shown by the solid black line and the dotted (red) line, respectively. The inset shows the detail of the plateaus from 300 to 400 eV. (b) Time-frequency distributions of the HHG corresponding to the case of $\varphi_1 = 0$, $\varphi_2 = 0.5\pi$.

the long path is greater when the harmonic order increases. We also investigate the attosecond pulse by superposing a bandwidth of 50 eV in the other ranges of the plateau area, and find that a main pulse with the duration of 75 as accompanied by a weak satellite pulse will be generated. Thus attosecond pulses with a tunable central wavelength would be generated for the case of $\varphi_1 = 0$, $\varphi_2 = 0.5\pi$. Because the intrinsic chirp attosecond pulse and the duration of the spectral generation is large (from about 4.80 to 5.35 optical cycle of 1600 nm), the duration of the attosecond pulse does not reach the Fourier limit 36 as.

In conclusion, we propose a scheme to control the quantum paths and IAP generation by synthesizing a left and a right circularly polarized Gaussian laser pulse with a proper time delay. When the carrier phases are $\varphi_1 = 0$, $\varphi_2 = 0.5\pi$, the "gating" structure of the combined laser field disappears, but this could control the interference of the quantum paths. The HHG process is investigated by the semiclassical three-step model that makes use of a finite initial transverse velocity in the elliptically polarized field. For the cases of $\lambda_1 = 800$ nm, $\lambda_2 = 1600$ nm and $\varphi_1 = 0$, $\varphi_2 = 0.5\pi$, only a short path contributes to the HHG, and an isolated attosecond pulse with a duration of 120 as could be obtained. When both the wavelengths are 1600 nm and $\varphi_1 = 0$, $\varphi_2 = 0.5\pi$, a supercontinuum plateau which includes the whole water window region is obtained, and there is only a photon energy peak A_5 contributing to the HHG from 220 to 570 eV. A main pulse with the duration of 75 as accompanied by a weak satellite pulse will be generated by superposing a bandwidth of 50 eV in the plateau area.

This work was supported by the National Natural Science Foundation of China (11174108 and 11271158). We also acknowledge the High Performance Computing Center (HPCC) of Jilin University for supercomputer time.

[1] F. Krausz and M. Ivanov, Rev. Mod. Phys. **81**, 163 (2009).
[2] P. B. Corkum, Phys. Rev. Lett. **71**, 1994 (1993).
[3] W. Hong, P. Lu, Q. Li, and Q. Zhang, Opt. Lett. **34**, 2102 (2009).
[4] Y. Zheng, Z. Zeng, R. Li, and Z. Xu, Phys. Rev. A **85**, 023410 (2012).
[5] E. Goulielmakis, M. Schultze, M. Hofsteter, V. S. Yakovlev, J. Gagnon, M. Uiberacker, A. L. Aquila, E. M. Gullikson, D. T. Attwood, R. Kienberger, F. Krausz, and U. Kleineberg, Science **320**, 1614 (2008).
[6] C. Altucci, V. Tosa, and R. Velotta, Phys. Rev. A **75**, 061401(R) (2007).
[7] E. J. Takahashi, P. Lan, O. D. Mucke, Y. Nabekawa, and K. Midorikawa, Phys. Rev. Lett. **104**, 233901 (2010).
[8] P. Lan, P. Lu, Q. Li, F. Li, W. Hong, and Q. Zhang, Phys. Rev. A **79**, 043413 (2009).
[9] H. Du, L. Luo, X. Wang, and B. Hu, Opt. Express **20**, 9713 (2012).
[10] S. F. Zhao, X. X. Zhou, P. C. Li, and Z. Chen, Phys. Rev. A **78**, 063404 (2008).
[11] C. L. Xia, G. T. Zhang, J. Wu, and X. S. Liu, Phys. Rev. A **81**, 043420 (2010).
[12] G. T. Zhang, J. Wu, C. L. Xia, and X. S. Liu, Phys. Rev. A **80**, 055404 (2009).
[13] P. B. Corkum, N. H. Burnett, and M. Y. Ivanov, Opt. Lett. **19**, 1870 (1994).
[14] Z. Chang, Phys. Rev. A **70**, 043802 (2004).
[15] Z. Chang, Phys. Rev. A **71**, 023813 (2005).
[16] Q. Zhang, P. Lu, P. Lan, W. Hong, and Z. Yang, Opt. Express **16**, 9795 (2008).
[17] Z. Chang, Phys. Rev. A **76**, 051403(R) (2007).
[18] H. Mashiko, S. Gilbertson, C. Li, S. D. Khan, M. M. Shakya, E. Moon, and Z. Chang, Phys. Rev. Lett **100**, 103906 (2008).
[19] X. Feng, S. Gilberston, H. Mashiko, H. Wang, S. D. Khan, and M. Chini, Phys. Rev. Lett **103**, 183901 (2009).
[20] H. Eichmann, A. Egbert, S. Nolte, C. Momma, B. Wellegehausen, W. Becker, S. Long, and J. K. McIver, Phys. Rev. A **51**, R3414 (1995).
[21] D. B. Milosevic, W. Becker, and R. Kopold, Phys. Rev. A **61**, 063403 (2000).
[22] D. B. Milosevic and W. Becker, Phys. Rev. A **62**, 011403(R) (2000).
[23] M. Moller, Y. Cheng, S. D. Khan, B. Zhao, K. Zhao, M. Chini, G. G. Paulus, and Z. Chang, Phys. Rev. A **86**, 011401(R) (2012).
[24] N. I. Shvetsov-Shilovski, S. P. Goreslavski, S. V. Popruzhenko, and W. Becker, Phys. Rev. A **77**, 063405 (2008).
[25] G. Sansone, Phys. Rev. A **79**, 053410 (2009).
[26] R. Kopold, D. B. Milosevic, and W. Becker, Phys. Rev. Lett. **84**, 3831 (2000).
[27] P. Antoine and B. Piraux, Phys. Rev. A **51**, R1750 (1995).
[28] D. G. Arbo, K. L. Ishikawa, K. Schiessl, E. Persson, and J. Burgdorfer, Phys. Rev. A **81**, 021403(R) (2010).